Chinese Chemical Letters 34 (2023) 107839

Contents lists available at ScienceDirect

Chinese Chemical Letters

journal homepage: www.elsevier.com/locate/cclet

Defect engineering of vanadium-based electrode materials for zinc ion battery

Ying Liu, Yi Liu, Xiang Wu*

School of Materials Science and Engineering, Shenyang University of Technology, Shenyang 110870, China

ARTICLE INFO

Article history:
Received 8 August 2022
Revised 10 September 2022
Accepted 20 September 2022
Available online 22 September 2022

Keywords:
Aqueous zinc ion batteries
Vanadium-based materials
Cathodel energy storage devices
Defect engineering

ABSTRACT

With the quick development of sustainable energy sources, aqueous zinc-ion batteries (AZIBs) have become a highly potential energy storage technology. It is a crucial step to construct desired electrode materials for improving the total performance of AZIBs. In recent years, considerable efforts have focused on the modification of vanadium-based cathode materials. In this review, we summarized defect engineering strategies of vanadium-based cathodes, including oxygen defects, cation vacancies and heterogeneous doping. Then, we discussed the effect of various defects on the electrochemical performance of electrode materials. Finally, we proposed the future challenges and development directions of V-based cathode materials.

1. Introduction

The double carbon strategy retards the pace of environmental pollution and the energy crisis [1,2]. Lithium-ion batteries (LIBs) have captured most of the electronics market due to their high energy density and durable cycle life [3–5]. However, the scarcity of lithium resources and the flammability of the electrolyte lead to the high cost and low safety. It promotes the research focus towards aqueous metal ion batteries (Na, K, Ca, Zn, Al and Mg) [6–12]. Multivalent metal-ion batteries are attractive owing to their multiple electron transfer reactions. Among them, aqueous zinc-ion batteries (AZIBs) consist of zinc metal anodes, aqueous electrolytes and limited cathode materials. The former possesses the abundant resources, a theoretical capacity of 820 mAh/g, and a redox potential of −0.76 eV (*vs.* standard hydrogen electrode) [13–16]. Nevertheless, AZIBs are still plagued by the inability to match suitable cathode materials [17–19].

To date, various electrodes have been explored, such as vanadium-based materials, manganese-based compounds, Prussian blue derivatives, organics and other transition metal compounds [20–26]. They are all capable of achieving reversible Zn ion storage after long-term cycles. Thereinto, organic composites are the emerging electrode materials in recent years. They are in the early stage of development. The exploitation of organic cathodes with excellent capacity and high voltage platform is the primary consideration. It is necessary to further study their structure and mechanism. Vanadium-based materials are featured by multiple V oxidation states and diverse crystal structures. The large interlayer distance facilitates rapidly the embedding and de-embedding of Zn ions [27]. However, commercial electrode materials cannot meet the requirements due to their large particle radius and small specific surface area. In order to bridge the gap between AZIBs and practical applications, it is crucial to enhance the electrochemical performance of batteries. Many optimization strategies have been proposed based on the modification of V-based compounds. For instance, Chen *et al.* [28] prepared a porous V_2O_5 nanofibers with an open layered structure. The assembled batteries deliver a capacity of 319 mAh/g at 0.02 A/g. After 500 cycles, they still maintain a capacity retention of 81%. Wu's group [29] designed ultrathin and amorphous V_2O_5 grown directly on graphene (A-V_2O_5/G). This unique structure facilitates the shortening of the diffusion path of zinc ions and improves the conductivity of the electrode. Zn/A-V_2O_5/G battery can retain 80% of initial capacity after 3500 cycles. This structural design effectively increases the cycle life of the battery, which can be attributed to the accelerated electrochemical kinetics.

In addition, defect engineering is also considered as a feasible strategy to tune the electronic properties of materials, mainly including vacancies and doping (Fig. 1). The former is an intrinsic defect caused by atoms or ions in the structure forming vacancy defects in the original lattice position due to thermal vibrations. The latter is the impurity atoms or ions embedded in the lattice

* Corresponding author.
E-mail address: wuxiang05@163.com (X. Wu).

https://doi.org/10.1016/j.cclet.2022.107839
1001-8417/

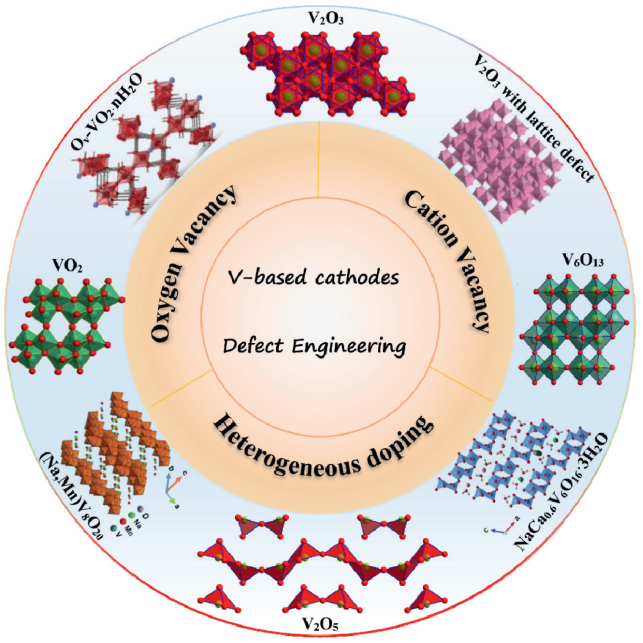

Fig. 1. A summary of defect engineering strategies for improving electrochemical performance of V-based electrode materials.

in the form of interstitial or replacement, which is a non-intrinsic defect [30]. The introduction of defects can effectively promote ion diffusion kinetics and improve electronic conductivity. Therefore, it is widely employed in the modification of electrode materials. Herein, we first summary recent advances in V-based electrode with different crystal structures. Then, we discuss the classification of defect engineering and focused on their effects on the electrochemical performance of vanadium-based materials through various strategies. Finally, we present the current challenges and future developments.

2. Defect engineering on V-based materials

2.1. Classification of V-based materials

Among many cathode materials, V-based compounds have captured much attention due to their low cost, and variety of crystal structures [31]. The valence state of vanadium ranges from +2 to +5. This rich oxidation state allows for multiple electron transfer and high theoretical capacity [32–34]. The crystal structure of vanadium oxides is determined by the coordination of V-O polyhedra and the oxidation state of V. From tetrahedron to square pyramids and triangular bipyramids, to distorted or regular octahedron, the varied structures provide multiple pathways for the transfer of zinc ions [35]. Fig. 2 shows the crystal structure of typical vanadium-based oxides. Based on the changes of valence, they can be categorized into two types: layered and tunnel structures. Among them, V_2O_5 materials are built by the deformed VO_5 square pyramid through the sharing of edges and corners to form a two-dimensional layered structure (Fig. 2a). The interlayer spacing is about 4.37 Å, which is favorable for the insertion of metal ions. For instance, Kundu *et al.* designed V_2O_5 materials with divalent Zn ions and H_2O intercalation ($Zn_{0.25}V_2O_5{\cdot}nH_2O$) as cathodes. The assembled cells deliver a capacity of 220 mAh/g at 15 C [36]. Alshareef's group prepared porous $Mg_{0.34}V_2O_5{\cdot}0{\cdot}84H_2O$ nanobelts materials. The large radius of the intercalation of hydrated Mg^{2+} (~4.3 Å) leads to an increase in the interlayer spacing to 13.4 Å. This facilitates the rapid insertion and extraction of Zn^{2+}. As a result, the prepared electrode achieves a capacity of 264 mAh/g at a current density of 1 A/g in a potential window of 0.1–1.8 V [37]. The intercalation of metal ions can not only stabilize the host structure but also enlarge the interlayer distance. This favors the increase of active sites and also weakens the strong interactions of zinc ion embedding.

As shown in Figs. 2b and c, VO_2 and V_2O_3 materials are tunnel structures composed of VO_6 octahedra sharing edges and corners. The former possesses a sufficient tunnel space (3.18 Å) than the latter (2.87 Å). In previous work [38], we reported VO_x@C microspheres as cathodes. Thereinto, VO_2@C electrodes show a stable cycling life after 1000 cycles and high rate capability. As a comparison, VO_2 and V_2O_3 electrode possess inferior specific capacity and cycle performance. It can be explained by the fact that the large tunneling space of VO_2 is more conducive to zinc ions. V_6O_{13} materials with open structure contain V^{5+}/V^{4+} mixed valence. Their crystal structure consists of alternating single and double [VO_6] octahedral layers (Fig. 2d). Liang's group [39] prepared V_6O_{13} cathode, which delivers a capacity of 206 mAh/g at 10 A/g after 3000 cycles. In addition, the zinc vanadate phase ($Zn_{0.25}V_2O_5{\cdot}H_2O$) appears during the embedding of zinc ions and recovers to the original phase when the Zn ions are extracted. The occurrence of this phase transition leads to the insertion of much Zn^{2+} into the host structure. Thus, Zn/V_6O_{13} batteries possess a high Zn ion storage capacity.

$V_3O_7{\cdot}H_2O$ ($H_2V_3O_8$) is a layered structure composed of VO_6 octahedron and VO_5 trigonal bipyramids. The V_3O_8 layers are linked together by hydrogen bonds, which can easily intercalate Zn ions (Fig. 2e). Compared with the above-mentioned materials, the presence of hydrogen bonds in $V_3O_7{\cdot}H_2O$ can provide excellent structural stability during repeated cycling. In addition, V^{5+} and V^{4+} co-exist in a 2:1 ratio in the structure, resulting in the high electronic conductivity. This suggests that it possesses more active redox sites. He and collaborators [40] reported the assembly of Zn cells using layered $H_2V_3O_8$ nanowires as cathodes and Zn anodes with a $Zn(CF_3SO_3)_2$ aqueous electrolyte. Benefiting from the large interlayer spacing, they can maintain an initial capacity of 94.3% after 1000 cycles. To further improve the cycle life, Pang *et al.* [41] designed a graphene sheet-wrapped $H_2V_3O_8$ nanowire electrode. The composite materials own a high specific surface area, which is beneficial to increase the contact area between the electrode and the electrolyte. At high current density (20 C), the electrode can run stably for 2000 cycles.

In Fig. 2f, the intercalation of water molecules between V_2O_5 layers plays a crucial role in expanding and supporting the layered framework of V_2O_5-based materials. Yang's group [42] prepared $V_2O_5{\cdot}nH_2O$/graphene (VOG) *via* a liquid phase approach. The results show that the electrostatic interaction between Zn^{2+} and V_2O_5 framework is weakened after water solvation, which effectively increases the diffusion rate of Zn^{2+}. Thus, H_2O acts as a charge shield for the intercalated metal ions during cycling, reducing their effective charge. Liang and co-workers [43] inserted Li^+ into the $V_2O_5{\cdot}nH_2O$ interlayer, widening the (001) plane spacing from 12.1 Å to 13.77 Å. $Zn/Li_xV_2O_5{\cdot}nH_2O$ (LVO) batteries present highly reversible rate performance and maintain a capacity of 192 mAh/g after 1000 cycles (10 A/g).

A variety of vanadium-based compounds formed with V-O layers as the main structure have been explored for AZIBs, but the unmodified electrodes still face many challenges in terms of electrochemical performance. In Fig. 3, the cell possesses a slow kinetic process due to the inherent poor conductivity of the V-base material as well as the strong electrostatic interactions when the carrier Zn^{2+} is embedded. In addition, the dissolution of the cathode promotes the formation of unfavorable by-products. These adverse effects are the crucial reasons for the decrease in the actual capacity of the electrode. For this reason, researchers have turned their attention to the modulation of materials structure.

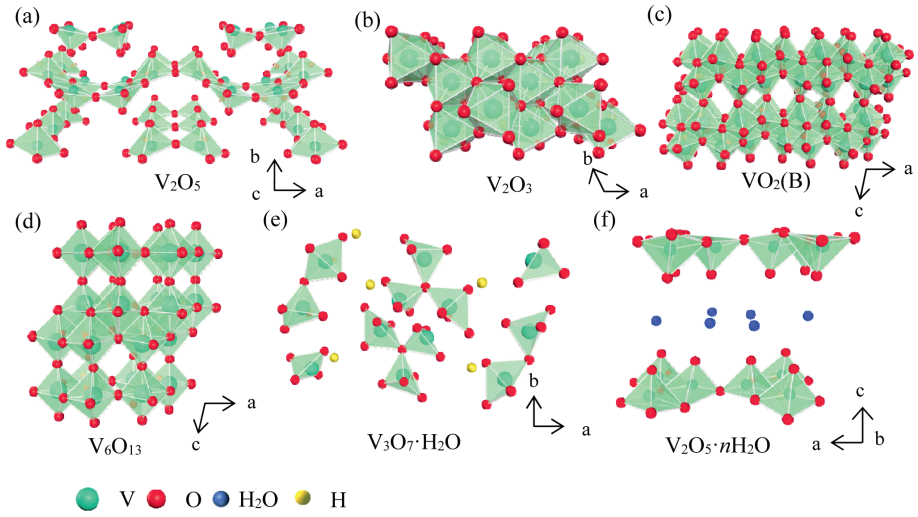

Fig. 2. The crystal structures of V-based oxides: (a) V_2O_5; (b) V_2O_3; (c) $VO_2(B)$; (d) V_6O_{13}; (e) $V_3O_7{\cdot}H_2O$; (f) $V_2O_5{\cdot}nH_2O$.

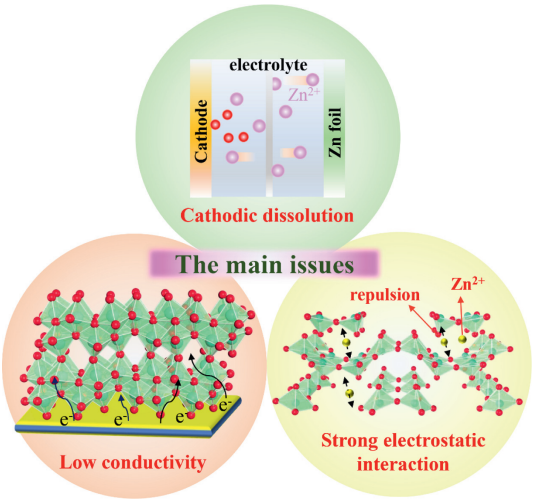

Fig. 3. The main issues of V-based electrode materials.

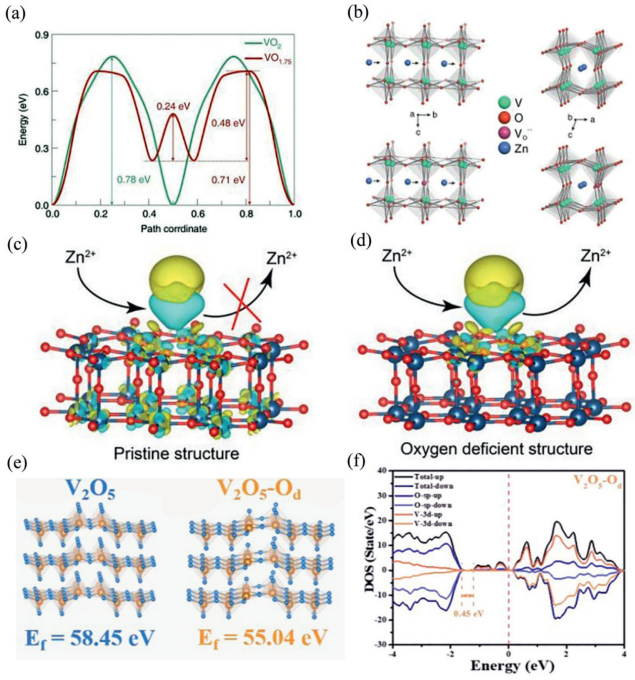

Fig. 4. DFT calculation of electrodes with V_o. (a) Zn ion diffusion energy barriers; (b) Zinc ions diffusion pathways along the b tunnel in VO_2 and $VO_{1.75}$ electrode. Reproduced with permission [49]. Copyright 2020, American Chemical Society. (c, d) Schematic of Zn^{2+} insertion/extraction for perfect and oxygen deficient vanadium oxide (O_d-VO), respectively. Reproduced with permission [50]. Copyright 2019, Wiley-VCH. (e) Calculated formation energy of two electrodes. (f) DOS of V_2O_5-O defects. Reproduced with permission [52]. Copyright 2021, Elsevier Ltd.

2.2. Effect of defects engineering on zinc ion storage capacity

2.2.1. Classification of defects

In the past decades, there has been the common strategies to improve electrochemical activity and electrical conductivity by introducing structural defects in target materials [44]. Defect engineering can change the surface chemistry, electronic structure or coordination mode of materials, which is widely used in various fields such as catalysis and energy storage [45,46]. Defects are of various types including vacancies (anions and cations), and heteroatom doping. In the field of AZIBs, these defects endow V-based materials with new capabilities in electronic, magnetic, and optical properties [47]. We will specifically discuss the effect of different defects on the energy storage performance of the cells in the following sections.

2.2.2. Anion vacancy

Oxygen vacancies (V_o) is a structural defect formed by the escape of an oxygen ion from the lattice. Their presence shortens the shuttle path of ions and causes an increase in the conductivity and diffusion coefficient of the material. Therefore, the fabrication of V_o plays an important role in the improvement of electrochemical performances such as specific capacity, energy density, and cycling stability of battery [48]. Cao's group [49] designed VO_2 materials with V_o and found that oxygen vacancies can enlarge the tunneling space of VO_2 electrode. Further, density functional theory (DFT) calculations confirm that the $VO_{1.75}$ electrode owns a narrow band gap. It suggests a low binding energy of valence electrons and enhanced charge transport. Fig. 4a also presents a lower diffusion energy barrier than the VO_2 electrode when the zinc ions are embedded into the structure. This indicates that the electrode with V_o possesses a rapid electrochemical kinetic process (Fig. 4b).

In fact, the batteries show inferior cycling stability when repeatedly cycled, especially at high current densities. Many ef-

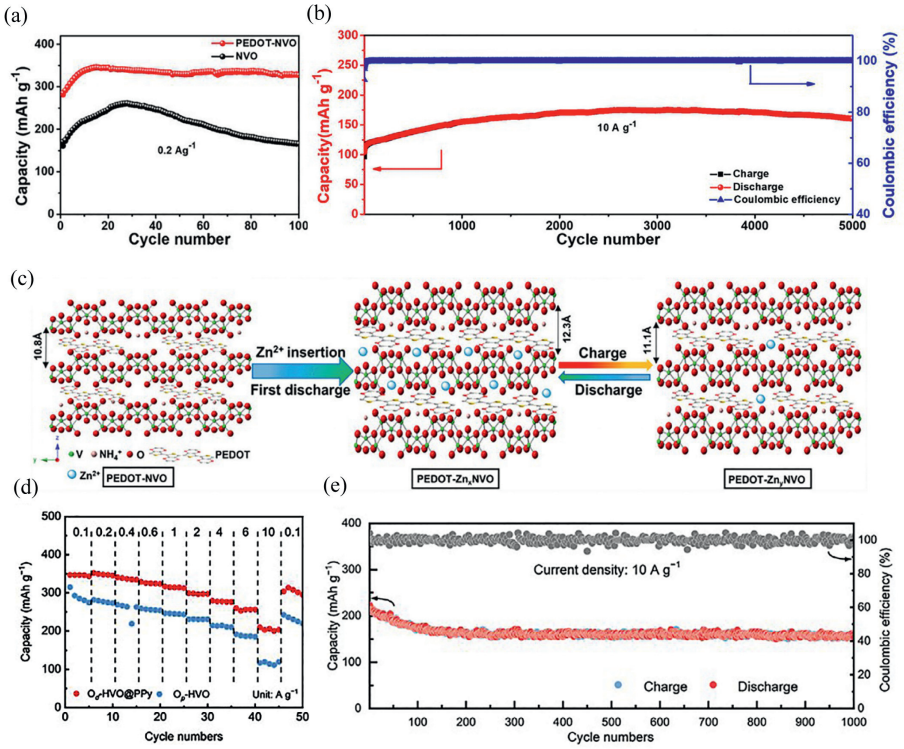

Fig. 5. The electrochemical performances of the electrode with V_o. (a) Cycling performance of the two cathodes at 0.2 A/g. (b) The long-term cycle capability. (c) The Zn^{2+} storage mechanism of Zn/PEDOT-NVO batteries. Reproduced with permission [56]. Copyright 2020, Elsevier Inc. (d) Rate capability at varying current densities. (e) Long life cycling performance. Reproduced with permission [57]. Copyright 2021, Wiley-VCH GmbH.

forts have been made to solve this issue. For instance, Liao *et al.* [50] prepared oxygen-deficient V_6O_{13} cathodes by a redox self-assembly method. In Figs. 4c and d, the partial absence of electronegative oxygen in the V_6O_{13} lattice can effectively improve the Zn^{2+} diffusion rate as well as the reversibility of charge and discharge. When the oxygen atoms are extracted, there are excess electrons to form defective sites, which contribute to the formation of delocalized electron clouds to increase the discharge capacity [51]. Also, the defect-free structure shows a higher Gibbs free energy of desorption than the defective electrode. This indicates that Zn ions are difficult to desorb, resulting in reduced cycling stability. As a result, the modified electrode materials deliver an initial capacity of 401 mAh/g at 0.2 A/g and a stable cycle of 2000 cycles at high current density (2 A/g). Qin and coworkers [52] introduced V_o into the main structure of V_2O_5 in order to overcome its slow dynamics. Based on DFT calculations, the defect optimizes the internal electronic structure of the electrode, providing a bandgap of 0.45 eV and lowering the Zn^{2+} diffusion energy barrier (0.72 eV) and generation energy (55.04 eV) in Figs. 4e and f. The cells can present a specific capacity of 427.3 mAh/g at 0.1 A/g and obtain a capacity retention of 92.1% after 5000 cycles.

The Gibbs free energy of zinc ion adsorption/desorption is an important parameter to assess the reversibility and kinetic process of zinc ion. In previous reports [53], the electrochemical kinetics of potassium vanadate cathodes were successfully optimized by combining oxygen vacancies with a carbon coating strategy. The synthesized oxygen-deficient potassium vanadate/amorphous carbon nanoribbons (C-KVO|O_d) possess low Zn^{2+} adsorption Gibbs free energy and energy barrier. It suggests a highly reversible Zn^{2+} adsorption/desorption process. Amorphous carbon facilitates the rapid transfer of electrons. Thus, this unique structure both improves the conductivity of the electrode and provides more active sites for Zn^{2+} storage. Benefiting from this synergistic effect, the C-KVO|O_d cathode presents a capacity of 385 mAh/g at 0.2 A/g and maintains a high capacity (160 mAh/g) at 20 A/g.

The creation of V_o in metal oxides can be achieved in several ways: (1) heat treatment in an inert atmosphere; (2) using a reducing agent to partially reduce the metal ions in the metal oxide during the reaction to generate V_o; (3) materials treated with plasma are in an electronically excited state with high energies, which is beneficial for the appearance of V_o; (4) carbonization of organic-containing reaction precursors. Note that oxygen vacancies can be formed in an oxygen barrier and high temperature environment; and (5) the lattice distortion caused by heterodoping forms V_o [54]. The first three routes are commonly used in the preparation of electrodes for rechargeable metal ions batteries [50,52,55].

Recently, a strategy is developed to introduce V_o *via* an *in-situ* polymerization process using conductive polymer. For example, Bin *et al.* [56] designed a layered $NH_4V_3O_8$ electrode with poly(3,4-ethylenedioxythiophene) (PEDOT) intercalation (PEDOT-NVO) to increase the interlayer spacing from 7.8 Å to 10.8 Å. The formation of oxygen vacancies is attributed to the polymerization of EDOT monomers and the reduction of V_3O_8 layers. Electron paramagnetic resonance (EPR) confirms the appearance of oxygen vacancies. Zn/PEDOT-NVO cells show an activation capacity of 345.5 mAh/g at 0.2 A/g and maintain a discharge capacity of 160.6 mAh/g after 5000 cycles (10 A/g, Figs. 5a and b). Moreover, their energy density can reach 353.1 Wh/kg at a power density of 50 W/kg (based on the mass of the cathode). In Fig. 5c, the absence of side reactions during the reaction process further reveals the zinc ion embedding/extracting mechanism. It corresponds to their long cycle life. Therefore, this is an effective strategy to introduce oxygen vacancies through the embedding of conducting polymers. A similar

electrode design is used by Xiong's group [57] to enhance the zinc storage capacity of vanadium dioxide. They fabricated the oxygen-free hydrate VO_2 with polypyrrole (PPy) coating (O_d-HVO@PPy) by simple one-step hydrothermal route. The polymer coating alleviates cathodic dissolution and enhances electron transfer. Moreover, the oxygen vacancies contribute to the reversible adsorption of Zn ions on the electrode surface. The incorporation of structured water can effectively regulate the electrostatic interactions of Zn^{2+} [58]. Abided by the proton and Zn ion co-embedding mechanism, the cell provides superior rate performance and cycling stability after 1000 cycles (a capacity of 159 mAh/g at 10 A/g), as shown in Figs. 5d and e.

In order to improve the conductivity of the electrode, besides introducing V_o, it is also a potential route to combine with high conductivity materials. Huang *et al.* [59] constructed a three-dimensional (3D) sponge-like hydrated VO_2 and graphene composite (O_d-HVO/rG) with abundant oxygen defects. The electrode presents a high specific capacity (428.6 mAh/g at 0.1 A/g), fast electrochemical kinetics, and long cycle life (197.5 mAh/g after 2000 cycles). Most electrodes are based on structural chemical defects to optimize electrochemical performance. Chen *et al.* [60] reported vanadium oxide electrodes with both physical and chemical defect structures to improve the storage performance of zinc ions. They synthesized vanadium oxide nanofibers (VCN) with a 3D porous structure by electrospinning. Polyacrylonitrile (PAN) as a raw material produces V_o and a large number of pores during the pyrolysis process. This abundant pore structure is favoring to increase the specific surface of the sample, while oxygen vacancies bring more active sites. Based on this dual effect, the specific capacity of the battery is effectively enhanced. The host structure of the 3D network can provide more diffusion paths for Zn ions, it facilitates rapid transfer of zinc ions.

2.2.3. Cation vacancy

The induction of defects creates more active sites than the limited diffusion of the original material. This can be used to accommodate additional reversible ion intercalation. Cation vacancies have also attracted some attention in multivalent metal secondary batteries because they can weaken electrostatic interactions during ion intercalation [61]. The construction of cationic defects requires an increase in the surface energy of the material due to the high defect formation energy of cations. Therefore, the synthetic strategy is of particular importance. Currently, several approaches are commonly employed to introduce cationic vacancies into transition metal chalcogenides (TMCs) including different valence cation replacement, anion substitution, electrochemical charging process and pH-controlled methods [62–65]. In AZIBs, the strategies are mostly used in the modification of Mn-based compounds [66,67]. In particular, spinel structured electrodes with strong lattice charge repulsion are unable to store Zn. For instance, Chen and co-workers designed a cation-deficient $ZnMn_2O_4$ cathode material. The introduction of Mn vacancies accelerates their electrochemical kinetics. The battery presents a superior rate performance and stable cycle capability of 500 cycles [68]. Therefore, the introduction of cationic vacancies is also an effective approach to improve the energy storage capacity. For vanadium-based compounds, there are still challenges in the exploration of cationic vacancy-modified electrodes.

Chou *et al.* [64] demonstrated *in situ* lattice distortion of V_2O_3 induced by the charging process. The prepared V-defect-rich V_2O_3 material is used as a cathode for Zn^{2+} storage. Fig. 6a shows that the energy required for zinc intercalation decreasing (from −0.28 eV to −0.72 eV) as the number of vacancies increase. It indicates that the abundant vanadium vacancies in V_2O_3 favor the Zn^{2+}insertion. *In situ* XRD further confirmed the structural changes of the electrodes during the first charge and subsequent cycling. The shift of the crystal planes is related to the insertion and extraction of zinc ions. Fig. 6b demonstrates the formation of lattice defects and zinc ion storage sites during charge/discharge. The *in situ* electrochemical lattice conversion strategy enables the electrode to achieve a capacity of 154.3 mAh/g at high current density (51.2 A/g).

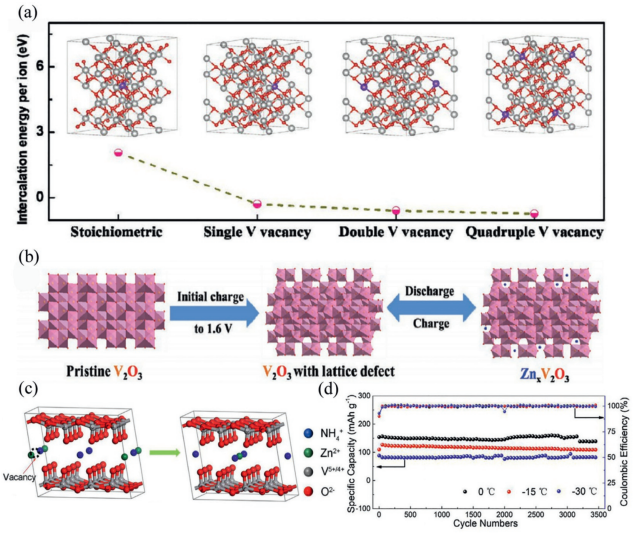

Fig. 6. The electrochemical performances of electrodes with cationic vacancies. (a) DFT calculated intercalation energies for zinc ions in V_2O_3 with different vacancies. (b) Schematic of the initial charging process for V_2O_3 and the subsequent Zn^{2+} storage process. Reproduced with permission [64]. Copyright 2021, Wiley-VCH. (c) Schematic of Zn^{2+} diffusion in the ZNV with NH_4^+ vacancies in the interlayers. (d) Low-temperature cycling performance at 2 A/g. Reproduced with permission [70]. Copyright 2021, Elsevier B.V.

Protective measures of cation pre-insertion into the host material can ensure the structural stability of the electrode during long-term cycling [69]. Notably, it is also possible to introduce cationic vacancies indirectly during the synthesis. He *et al.* [70] designed the $Zn_{0.3}(NH_4)_{0.3}V_4O_{10}{\cdot}0{\cdot}91H_2O$ (ZNV) cathode with abundant cation vacancies. DFT calculations show that the pre-intercalation of Zn^{2+} leads to the formation of four different defects in the structure including NH^{4+}, V_1, V_2 and $Zn^{2+}/V^{5+/4+}$ cationic vacancies, as presented in Fig. 6c. The Zn^{2+} diffusion barrier of defective ZNV electrodes is significantly lower than that of non-defective ones. This suggests that the existence of defects is conducive to the rapid diffusion of zinc ions between layers. Thereinto, the NH^{4+} vacancies can obtain the energy barrier of 0.862 eV than other defects. The results show that ZNV electrodes deliver a discharge capacity of 461.1 mAh/g (0.1 A/g). And there is almost no decay after 2000 cycles at 2 A/g. In addition, stable cycling performance and long cycle life (3500 cycles) are still obtained under extreme temperature conditions (0, −15 and 30 °C, Fig. 6d). Thus, the cation vacancies caused by Zn^{2+} pre-intercalation are essential to improve the migration rate of Zn^{2+} in the electrolyte and to assure a superior reaction kinetics of ZNV in a wide temperature range.

The quantitative analysis of defects is crucial to identify metal vacancies and V_o in the materials. The Rietveld refinement of XRD technique is often employed to quantify the defect concentrations. However, the presence of V_o is generally difficult to be captured by XRD pattern due to the small atomic radius. Therefore, Rietveld refinement of neutron powder diffraction (NPD) is more suitable for light and small elements. Zhu and collaborators [71] combined two techniques to quantify V-deficient V_2O_3 (V_d-V_2O_3) electrodes with 5.7% V_d clusters. The XANES (X-ray absorption near edge structure) spectra of V K-edge detected defects in the V_2O_3 sample, as shown in Fig. 7a (Site A). The pre-edge peak intensity of the ma-

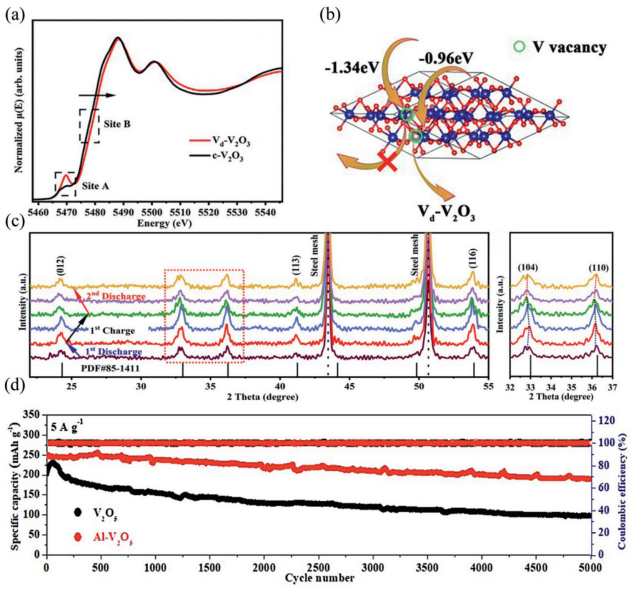

Fig. 7. The kinetics process and the cycling performance. (a) The XANES spectra of V K-edge. (b) The Gibbs free energy. (c) *Ex situ* XRD patterns of V_d-V_2O_3 electrodes at different cut-off voltages during the charge and discharge process. Reproduced with permission [71]. Copyright 2021, Springer Nature. (d) Cycling stability of the electrodes at 5 A/g. Reproduced with permission [79]. Copyright 2022, Elsevier B.V.

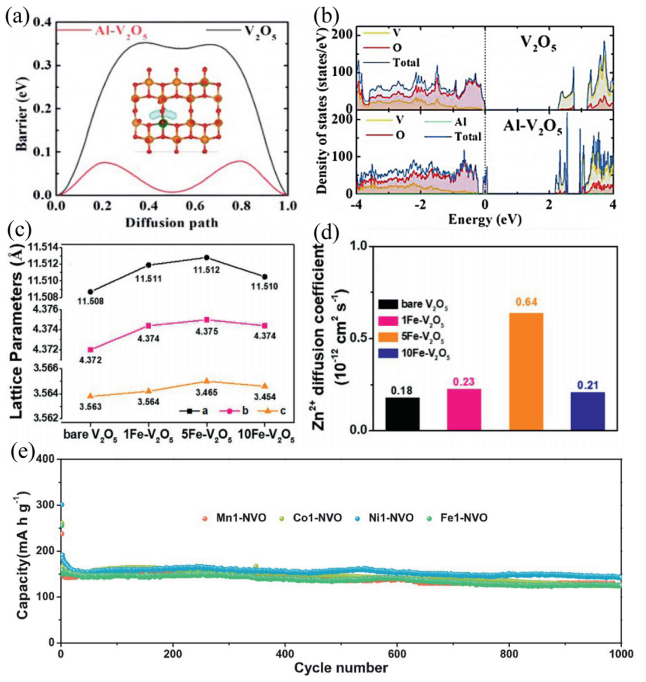

Fig. 8. DFT calculation and the cycle capability of electrode with ion doping. (a) Energy barriers for diffusion paths in two electrodes. (b) DOS of the two samples. Reproduced with permission [79]. Copyright 2022, Elsevier B.V. (c) Lattice parameters and (d) the zinc-ion diffusion coefficient of samples. Reproduced with permission [81]. Copyright 2021, Elsevier B.V. (e) Cycle performance at a current rate of 4 A/g. Reproduced with permission [83]. Copyright 2020, Wiley-VCH.

terial is significantly enhanced compared to the defect-free sample. It indicates that the structure of V_d-V_2O_3 is distorted around the V atoms, which can be attributed to the absence of surrounding atoms. As shown in Fig. 7b, the insertion of Zn^{2+} into V_d-V_2O_3 structure shows different Gibbs free energies. Zn ions occupy vanadium vacancies, which can release −1.34 eV heat under strong electrostatic interaction. It reinforces the stability of the host structure. However, the extraction of Zn^{2+} becomes difficult undergoing this strong interaction. Part of the Zn^{2+} is riveted on the vanadium vacancies, resulting in the residue of Zn. It can be observed the expansion and contraction of the V_d-V_2O_3 lattice with the intercalation and de-intercalation of Zn^{2+} in the *ex situ* XRD patterns (Fig. 7c). The 5.7% V_d clusters accelerate the diffusion of Zn ions. The battery can be repeatedly charged and discharged 30,000 times with the capacity retention of 81%.

2.2.4. Heterogeneous doping

Typical heteroatom doping includes metallic and non-metallic doping. For the former, metals such as Li, Na, K, Al, and Co are used for interlayer doping [43,57,72,73] Mai's group [74] reported Na^+ intercalation between V_2O_5 layers as cathode. The Zn/$Na_{0.33}V_2O_5$ battery obtains a stable structure and keeps a capacity of 93% for 1000 cycles. Other alkali metals with larger atomic radii have also been explored, which are hindered in terms of specific capacity despite improved structural stability [75,76].

For electrode materials, the limited ion diffusion path is one of the main factors leading to their performance degradation. During the reaction, the diffusion of carriers is hampered, which causes severe structural deformation and irreversible reactions. Therefore, the pre-intercalated metal ions can act as "pillars" and expand the interlayer space of vanadium oxide. This type of intercalation not only increases the stability of the crystal structure, but also optimizes electrical conductivity of electrode. It contributes to the stable intercalation of Zn ions and enhances its energy storage capacity.

Cationic doping can generally be divided into substitutional and interstitial doping. Jo *et al.* [72] prepared a hollandite-type $VO_{1.52}(OH)_{0.77}$ material with tunnel structure and introduced Al element in the host structure. They found that Al^{3+} ions replace part of the V ions, which can be represented by $V_{1-x}Al_xO_{1.52}(OH)_{0.77}$ ($x = 0$, 0.05, and 0.09). Since the radius of Al^{3+} (0.535 Å) is smaller than that of V ions ($V^{3+} = 0.64$ Å, and $V^{4+} = 0.58$ Å) [77], the linear decrease of lattice parameters is consistent with Vegard's law. Compared with $VO_{1.52}(OH)_{0.77}$, the doping of Al stabilizes the electrode structure, which is beneficial to the enhancement of the cycle performance. Wang's group [78] reported the doping of Al in layered $V_{10}O_{24}$ materials to maintain the stability of the crystal structure. Pure $V_{10}O_{24}$ electrode possesses a high initial specific capacity, but their capacity declines rapidly with increasing number of cycles. As a comparison, Al-doped $V_{10}O_{24}$ electrode achieves a positive influence in the electrochemical performance. Specifically, they can charge and discharge stably up to 3000 cycles and maintain 98% of the capacity.

Similarly, Jiang and collaborators [79] developed a high-temperature quenching approach to introduce Al ions into the V_2O_5 interlayer and form abundant V_o on the electrode surface. Benefiting from the participation of these defects, the optimized electrode material shows a long cycle life (5000 cycles) and excellent rate capability (Fig. 7d). The influence of Al doping on the electronic properties of the host material is further evaluated by DFT calculations. From Fig. 8a, it can be shown that Al is suitable to replace the vertex position from the energy point of view. Furthermore, the addition of Al and the formation of V_o reduces the diffusion barriers of Zn (0.36 eV drops to 0.09 eV). It indicates that doping can accelerate the reaction kinetics of the electrode. The density of states in Fig. 8b further confirms that the conductivity of the electrode material is effectively improved. The presence of oxygen vacancies induces changes in electrochemical activity and local rearrangement of the electronic structure, which promotes the accumulation of charge carriers [80].

The doping of metal ions can effectively change the geometrical structure of the material, including the adjustment of layer spacing and rearrangement. Therefore, it can positively affect the electrical

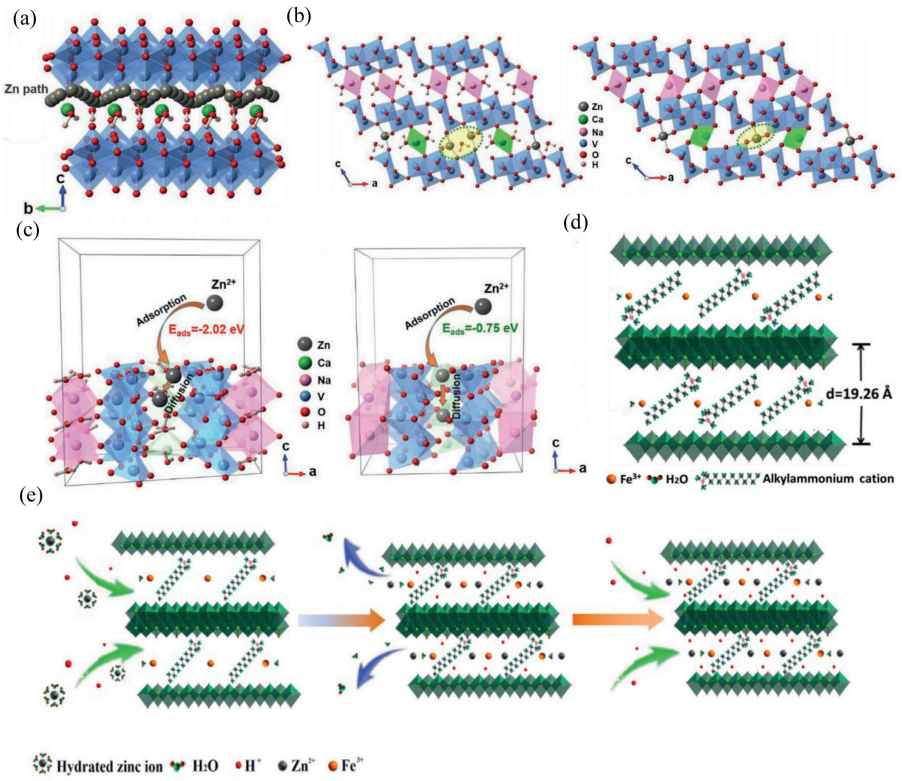

Fig. 9. The kinetic process of dual ion-doped V-based electrodes. (a) Migration path of Zn^{2+} in NaCaVO along the *b*-axis. (b) The crystal structure of NaCaVO and NaCaVO with no structural water electrodes after Zn-ions intercalation. (c) Zn^{2+} adsorption and diffusion models from surface to bulk. Reproduced with permission [84]. Copyright 2019, Wiley-VCH. (d) The crystal structure of iron ion and alkylammonium cation co-intercalated vanadium oxide. (e) Schematic of the energy storage mechanism. Reproduced with permission [85]. Copyright 2022, Elsevier B.V.

conductivity, ion diffusion rate, and structural stability of the material. Yoo *et al.* [81] prepared Fe-doped V_2O_5 nanorods samples by electrospun polyacrylonitrile (PAN) fibers template and annealing at high temperature. To investigate the effect of the amount of Fe doping on V_2O_5, they synthesized various Fe-V_2O_5 materials. The successful doping of Fe ions can be confirmed by the change of lattice parameters. From Fig. 8c, all lattice parameters of V_2O_5 material gradually expand with increasing amount of Fe source. This may be attributed to the formation of FeO_6 octahedra between the V_2O_5 layers. Additional active sites are provided for the storage of Zn ions. The occupation of V^{5+} sites by Fe^{3+} also generates oxygen vacancies, causing an increase in electrode conductivity. Among them, 5Fe-V_2O_5 sample possesses a high Zn ion diffusion coefficient (Fig. 8d), which may be due to the narrowing of the bandgap. Therefore, the optimized electrode can deliver a capacity of 422 mAh/g at 0.5 A/g and maintain a capacity retention of 85% after 160 cycles at 1.3 A/g.

The layers in $V_2O_5{\cdot}H_2O$ are connected by hydrogen bonds. This is similar to the structure of the $H_2V_3O_8$ material, as shown in Figs. 2e and f. Previous studies [36,37] have confirmed that the introduction of metal ions between the V_2O_5 layers can lead to improved cycling stability. Inspired by this, the researchers began to develop the doping of the V_3O_8 layer. Compared with monovalent cations (Na^+, Li^+), the introduction of polyvalent ones results in strong ionic bonds. It can suppress lattice distortion during cycling [82].

Adding divalent cations to the V_3O_8 layer is also one of the directions to stabilize cycling and prolong lifetime. Liu's group [83] added Mn ions to the NaV_8O_{20} material to improve its conductivity. With the combined effect of monovalent and divalent ions, $(Na_{0.33},Mn_{0.65})V_8O_{20}{\cdot}nH_2O$ materials maintain a stable cycle for 1000 cycles with a capacity loss of 1%. To study the role of Mn ions, they replaced new transition metal materials, such as Fe, Co, Ni, Ca, for comparison. The results show that the capacity retention of other electrodes is significantly lower than that of the Mn-optimized samples (Fig. 8e). This is mainly ascribed to the inhibition of electrode dissolution by the incorporation of Mn ions. Zhu *et al.* [84] reported the co-intercalation of monovalent and divalent metal cations into the V_3O_8 structure to form $NaCa_{0.6}V_6O_{16}{\cdot}3H_2O$ (NaCaVO) samples. The battery can deliver a capacity of 231 mAh/g after 2000 cycles. From Fig. 9a, the zinc ion diffusion path is further investigated by the *quasi*-empirical bond-valence (BV) approach. The embedded Zn^{2+} diffuses mainly in a zigzag shape along the *b*-axis. Structural water plays a crucial role in NaCaVO samples. The spacing of the V_3O_8 layers of the NaCaVO sample without crystal water is reduced from 8.1 Å to 6.7 Å (Fig. 9b). First, zinc ions possess low energy barriers at multiple diffusion paths. Then, sufficient interlayer space is favorable to the improvement of the storage capacity of Zn^{2+}. Then, structural water can reduce the Gibbs free energy of Zn absorption (−2.02 eV), which acts as a buffer against the strong electrostatic interaction of Zn ion (Fig. 9c). The Zn/NaCaVO battery can last for 10,000 cycles and retain a specific capacity of 125 mAh/g. This is the result of Na^+ and Ca^{2+} co-stabilizing the structure.

Considering the design of electrodes can combine the two roles of expanding the layer spacing and stabilizing the layer structure. Luo's group [85] explored the co-insertion of metal ions (iron ion) and organic molecules (alkylammonium cation) into layered vanadium oxide (FeVO-X) as cathodes. Among them, the intercalation of metal ions can generate strong electrostatic attraction between VO_x layers, which stabilizes the interlayer structure. The organic molecules can act as a role in expanding the interlayer spacing. It is favorable to increase the storage sites of Zn^{2+}. The optimal interlayer spacing can be obtained by adjusting the length (X) of

the alkyl chain in the alkylammonium cation. As shown in Fig. 9d, FeVO-12 samples possess an interlayer spacing of 19.26 Å. The assembled batteries deliver a specific capacity of 408 mAh/g at 0.1 A/g and can be charged and discharged stably up to 1000 times at 10 A/g. In addition, the charge storage mechanism of this electrode is further confirmed through *ex situ* XRD patterns and XPS spectra (Fig. 9e). The above double metal ion co-doping strategies can effectively optimize the electrode material structure from the following aspects. First, the enhancement of the electrical conductivity facilitates the rapid transfer of charges. Second, the widening of the layer spacing is beneficial in providing abundant Zn ion transport paths. Finally, the stable V-O layer prevents the main structure of the electrode from collapsing during repeated cycles.

Anion doping (such as N, P, S, C and Br) is also an efficient approach to further enhance the electrochemical performance of V-based materials. In previous reports, it has been revealed that the non-metallic heteroatoms can boost the ion transfer ability and promote the wettability of electrodes and electrolytes [86]. The replacement of highly electronegative oxygen with low electronegative elements such as N, S and C can reduce the diffusion barriers of Zn^{2+} in the structure. For instance, Wang *et al.* [87] synthesized the sandwich-like sulfur-doped V_2O_5/reduced graphene oxide/sulfur-doped V_2O_5 (S-V_2O_5/rGO) core-shell structure *via* a hydrothermal and calcination strategy. The results show that the Zn//S-V_2O_5/rGO battery delivers a specific capacity of 467 mAh/g at 0.4 A/g. And they can still obtain a capacity of 442 mAh/g at 2 A/g, demonstrating their excellent rate capability. This S-doped structure is beneficial to improve the electrical conductivity of the composites and promote the rapid transfer of Zn^{2+} and electrons. In addition, the design of the sandwich structure can provide abundant transport channels for Zn ions. Ge *et al.* [88] controlled the directional growth of the LiV_3O_8 material by doping with different amounts of bromine ions to form small rod-like particles (LVOB). The doping of Br ions presents some influence on the morphology of the samples. The ion doping behavior inhibits the directional growth and eventually leads to irregular change. In addition, their growth is accompanied by the evolution of defects, thus expanding the energy distribution for rapid redox reactions [89]. During the reaction, the charge imbalance causes the generation of oxygen defects. Notably, it is very critical to tune the appropriate content of doping elements for the enhanced zinc storage capacity. The introduction of excess Br ions reduces the stability and electrochemical activity of the cell. After 500 cycles, the optimized LVOB-2 electrode can maintain a capacity of 207 mAh/g, demonstrating its durable cycling stability. As a result, the excellent electrochemical performance is attributed to heteroatom doping and the generation of oxygen defects. So far, there are few literatures on anion doping with V-based compounds as host materials. This also provides a direction for further exploration.

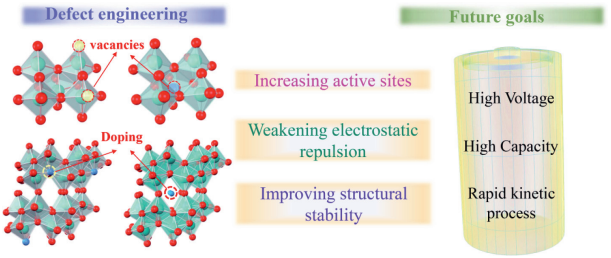

Fig. 10. The advantages of defect engineering and future goals for electrode materials.

3. Summary and outlook

In summary, vanadium-based electrodes perform unsatisfactorily in electrochemical performance for AZIBs due to their narrow operating voltage, electrode dissolution, sluggish electrochemical kinetics, and low electrical conductivity. Defect-rich materials can alter the atomic structure and charge distribution of the sample. The advantages of defect engineering in electrode materials can be described as follows (Fig. 10): First, the defects induce more active sites, effectively improving the specific capacity of the battery. Secondly, they can weaken the strong electrostatic interaction when zinc ions are embedded and promote the rapid charge transfer. Finally, the main structure can be stabilized to ensure the cycle life of the battery.

In Table 1, we summary the electrochemical performance of the vanadium-based electrode materials. It can be observed that the electrochemical stability and cycle life are greatly improved. The optimum electrode can maintain stable charge and discharge after 10,000 cycles. Therefore, the defect engineering strategy is an efficient and feasible way to solve the above problems. However, it is worth noting that these modifications cannot broaden the working voltage of the battery. Among various strategies to modify cathode materials, the modulation of electron cloud density can improve the electrochemical stability of organic sulfide compounds. A high voltage window of 1.7 V is achieved, which is superior to most V- and Mn-based compounds. Nevertheless, the electrochemical performance of the cathodes still fails to meet the market requirements. Hence, the development and exploration of electrode materials still face a large number of challenges.

In future work, we should first explore some ways to increase the energy density of batteries. For cathode materials, the capabil-

Table 1
The electrochemical performance of the optimized vanadium-based electrode materials.

Cathodes	Defect category	Methods	Voltage (V)	Capacity (mAh/g)	Cycle stability	Ref.
VO_2 (B)	Oxygen vacancies	Phase transition	0.3–1.5	375 (0.1 A/g)	85% after 2000 cycles (5 A/g)	[49]
V_6O_{13}	Oxygen vacancies	Thermal treatment	0.2–1.5	410 (0.2 A/g)	86% after 2000 cycles (2 A/g)	[50]
V_2O_5	Oxygen vacancies	Thermal reduction	0.4–1.5	427.3 (0.1 A/g)	92.1% after 5000 cycles (20 A/g)	[52]
$K_2V_8O_{21}$	Oxygen vacancies	Solid-state sintering	0.1–1.7	385 (0.2 A/g)	95% after 1000 cycles (3 A/g)	[53]
PEDOT-$NH_4V_3O_8$	Oxygen vacancies	Conducting polymer intercalation	0.4–1.6	356.8 (0.05 A/g)	94.1% after 5000 cycles (10 A/g)	[56]
V_2O_3	Vanadium vacancies	*In situ* electrochemical lattice conversion reaction	0.2–1.6	328 (0.8 A/g)	97.3% after 800 cycles (51.2 A/g)	[64]
$Zn_{0.3}(NH_4)_{0.3}V_4O_{10}{\cdot}0.91H_2O$	Cation-deficient	Hydrothermal method	0.1–1.9	461.1 (0.1 A/g)	100% after 2000 cycles (2 A/g)	[70]
Al-doped $V_{10}O_{24}{\cdot}12H_2O$	Heteroatoms doping	Hydrothermal method	0.3–1.6	355 (1 A/g)	98% after 3000 cycles (5 A/g)	[78]
$(Na,Mn)V_8O_{20}{\cdot}nH_2O$	Heteroatoms doping	Hydrothermal method	0.3–1.25	363 (0.1 A/g)	88% after 1000 cycles (4 A/g)	[83]
$NaCa_{0.6}V_6O_{16}{\cdot}3H_2O$	Heteroatoms doping	Hydrothermal method	0.4–1.5	347 (0.1 A/g)	83% after 10,000 cycles (5 A/g)	[84]
S-V_2O_5/rGO	Heteroatoms doping	Hydrothermal and calcination method	0.2–1.5	610 (0.1 A/g)	251 mAh/g after 1000 cycles (5 A/g)	[87]
Br-doped LiV_3O_8	Heteroatoms doping	Rheological phase method	0.2–1.6	247 (0.5 A/g)	207 mAh/g after 500 cycles (3 A/g)	[88]

ity of large capacity and high voltage together determines the energy density. There are several thinking directions: (1) The mass loading of electrode materials. Active substance mass is closely related to specific capacity. In the current reports, the loading of cathode materials is generally lower than 2 mg, which is not matched with the excessive Zn anode. The electrodes with high loading mass are closer to practical applications. However, it may lead to a reduction of specific capacity. (2) Increasing the operating voltage of the battery. The V-based polyanionic compounds show high working voltages beyond 1.2 V but suffer from inferior specific capacity. It is possible to modify their surface structural to improve the electrochemical performance. Also, it is a feasible approach to pre-insertion of high-potential transition metal ions into electrode materials.

Then, oxygen vacancy and cation doping are commonly used in defect engineering strategies. The optimal concentration of defects in the host structure for Zn ion storage has rarely been studied. Moreover, the variation of defects in the structure during charging and discharging needs to be further explored. *In situ* characterization approaches (XRD, XPS, *etc.*) facilitate the investigation of elemental evolution. At present, there are few studies on anion doping. Mn-based cathode materials are modified by this strategy to inhibit Mn ion dissolution accompanied by the formation of oxygen vacancies. This suggests that the introduction of anions (S, N, and F) into vanadium-based compounds is a promising direction. The changes caused by defects are mainly directed to the electronic structure and ion diffusion behavior. However, not all defects play a positive role. Researchers need to employ advanced characterization techniques to analyze the role played by defects and reduce the occurrence of negative effects.

Finally, the construction of defects can create more active sites and accelerate electrochemical kinetic processes. This optimized electrode can be composited with other materials including graphene, carbon nanotubes, conductive polymers to further enhance the conductivity. Furthermore, the appropriate modification on the surface defects of electrode materials can effectively modulate the electron interaction, local ion concentration, and energy storage behavior. The rational design of the electrode structure is an indispensable step in the development of high-performance cathode materials.

Declaration of competing interest

The authors declare that they have no known competing financial interests or personal relationships that could have appeared to influence the work reported in this paper.

Acknowledgment

The work is supported by National Natural Science Foundation of China (No. 52172218).

References

[1] J.B. Goodenough, Energy Storage Mater. 1 (2015) 158–161.
[2] D.P. Zhao, M.Z. Dai, Y. Zhao, et al., Nano Energy 72 (2020) 104715.
[3] J.M. Tarascon, M. Armand, Nature 414 (2001) 359–367.
[4] S. Ni, J. Liu, D. Chao, et al., Adv. Energy Mater. 9 (2019) 1803324.
[5] C. Liu, X. Wu, B. Wang, Chem. Eng. J. 392 (2020) 123651.
[6] S. Chen, C. Wu, L. Shen, et al., Adv. Mater. 29 (2017) 1700431.
[7] Q. Zhang, Z. Wang, S. Zhang, et al., Electrochem. Energy Rev. 1 (2018) 625–658.
[8] Y. Liu, X. Wu, J. Energy Chem. 56 (2021) 223–237.
[9] J. Zhang, Z. Chang, Z. Zhang, et al., ACS Nano 15 (2021) 15594–15624.
[10] M. Jiang, C. Fu, P. Meng, et al., Adv. Mater. 34 (2022) 2102026.
[11] S. Ye, L. Wang, F. Liu, et al., eScience 1 (2021) 75–82.
[12] B. Xu, S. Qi, F. Li, et al., Chin. Chem. Lett. 31 (2020) 217–222.
[13] Y. Liu, Y. Liu, X. Wu, Chem. Record. (2022) e2200088.
[14] M. Song, H. Tan, D. Chao, H.J. Fan, Adv. Funct. Mater. 28 (2018) 1802564.
[15] H.F. Li, L.T. Ma, C.P. Han, et al., Nano Energy 62 (2019) 550–587.
[16] Y. Liu, Y. Liu, Y. Yamauchi, et al., Batteries Supercaps 4 (2021) 1867–1873.
[17] B.Y. Tang, L.T. Shan, S.Q. Liang, J. Zhou, Energy Environ. Sci. 12 (2019) 3288–3304.
[18] Y. Liu, X. Wu, Chin. Chem. Lett. 33 (2022) 1236–1244.
[19] L.E. Blanc, D. Kundu, L.F. Nazar, Joule 4 (2020) 771–799.
[20] D. Selvakumaran, A. Pan, S. Liang, et al., J. Mater. Chem. A 7 (2019) 18209–18236.
[21] H. Liang, Z. Cao, F. Ming, et al., Nano Lett. 19 (2019) 3199–3206.
[22] Q. Yang, F. Mo, Z. Liu, et al., Adv. Mater. 31 (2019) 1901521.
[23] C. Luo, L. Xiao, X. Wu, CrystEngComm 24 (2022) 1387–1393.
[24] N. Li, G. Qu, X. Zhang, et al., Chin. Chem. Lett. 33 (2022) 3272–3276.
[25] H. Cui, T. Wang, Z. Huang, et al., Angew. Chem. Int. Ed. 61 (2022) e202203453.
[26] Z. Chen, H. Cui, Y. Hou, et al., Chem 8 (2022) 2204–2216.
[27] J. Ding, H. Gao, D. Ji, et al., J. Mater. Chem. A 9 (2021) 5258–5275.
[28] X. Chen, L. Wang, H. Li, et al., J. Energy Chem. 38 (2019) 20–25.
[29] X. Wang, Y. Li, S. Wang, et al., Adv. Energy Mater. 10 (2020) 200081.
[30] Y. Zhang, L. Tao, C. Xie, et al., Adv. Mater. 32 (2020) 1905923.
[31] X. Chen, H. Zhang, J.H. Liu, et al., Energy Storage Mater. 50 (2022) 21–46.
[32] C. Luo, L. Xiao, X. Wu, Mater. Adv. 3 (2022) 604–610.
[33] P. Ruan, S. Liang, B. Lu, et al., Angew. Chem. Int. Ed. 61 (2022) 202200598.
[34] K. Li, Y. Liu, X. Wu, CrystEngComm 24 (2022) 5421–5427.
[35] S. Zhang, H. Tan, X. Rui, et al., Acc. Chem. Res. 53 (2020) 1660–1671.
[36] D. Kundu, B.D. Adams, V. Duffort, et al., Nat. Energy 1 (2016) 16119.
[37] F.W. Ming, H.F. Liang, Y.J. Lei, et al., ACS Energy Lett. 3 (2018) 2602–2609.
[38] Y. Liu, Y. Liu, X. Wu, et al., ACS Appl. Mater. Interfaces 14 (2022) 11654–11662.
[39] L. Shan, J. Zhou, W. Zhang, et al., Energy Technol. 7 (2019) 1900022.
[40] P. He, Y. Quan, X. Xu, et al., Small 13 (2017) 1702551.
[41] Q. Pang, C. Sun, Y. Yu, et al., Adv. Energy Mater. 8 (2018) 1800144.
[42] M. Yan, P. He, Y. Chen, et al., Adv. Mater. 30 (2018) 1703725.
[43] Y. Yang, Y. Tang, G. Fang, et al., Energy Environ. Sci. 11 (2018) 3157–3162.
[44] Z. Liu, L. Qin, X. Cao, et al., Prog. Mater. Sci. 125 (2022) 100911.
[45] R.E. John, A. Chandran, M. Thomas, et al., Appl. Surf. Sci. 367 (2016) 43–51.
[46] Z. Duan, X. Tan, Y. Sun, et al., ACS Appl. Nano Mater. 4 (2021) 10791–10798.
[47] T. Xiong, Y. Zhang, W.S.V. Lee, J. Xue, Adv. Energy Mater. 10 (2020) 2001769.
[48] Y. Wang, X. Xiao, Q. Li, et al., Small 14 (2018) 1802193.
[49] Z. Li, Y. Ren, L. Mo, et al., ACS Nano 14 (2020) 5581–5589.
[50] M. Liao, J. Wang, L. Ye, et al., Angew. Chem. Int. Ed. 59 (2020) 2273–2278.
[51] G. Fang, J. Zhou, A. Pan, et al., ACS Energy Lett. 3 (2018) 2480–2501.
[52] J. Cao, D. Zhang, Y. Yue, et al., Mater. Today Energy 21 (2021) 100824.
[53] W. Yang, L. Dong, W. Yang, et al., Small Methods 4 (2019) 1900670.
[54] R. Wei, Y. Lu, Y. Xu, Sci. China Chem. 64 (2021) 1826–1853.
[55] G. Zhang, T. Xiong, M. Yan, et al., Nano Energy 49 (2018) 555–563.
[56] D. Bin, W. Huo, Y. Yuan, et al., Chem 6 (2020) 968–984.
[57] Z. Zhang, B. Xi, X. Wang, et al., Adv. Funct. Mater. 31 (2021) 2103070.
[58] Y. Liu, X. Wu, Nano Energy 86 (2021) 106124.
[59] S. Huang, S. He, H. Qin, et al., ACS Appl. Mater. Interfaces 13 (2021) 44379–44388.
[60] Z. Chen, J. Hu, S. Liu, et al., Chem. Eng. J. 404 (2021) 126536.
[61] J. Ma, T. Koketsu, B.J. Morgan, et al., Chem. Commun. 54 (2018) 10080–10083.
[62] T. Koketsu, J. Ma, B.J. Morgan, et al., Nat. Mater. 16 (2017) 1142–1148.
[63] W. Li, D. Corradini, M. Body, et al., Chem. Mater. 27 (2015) 5014–5019.
[64] J. Ding, H. Zheng, H. Gao, et al., Adv. Energy Mater. 11 (2021) 2100973.
[65] P. Gao, P. Metz, T. Hey, et al., Nat. Commun. 8 (2017) 14559.
[66] C. Zhu, G. Fang, S. Liang, et al., Energy Storage Mater. 24 (2020) 394–401.
[67] Y. Zhang, S. Deng, M. Luo, et al., Small 15 (2019) 1905452.
[68] N. Zhang, F. Cheng, Y. Liu, et al., J. Am. Chem. Soc. 138 (2016) 12894–12901.
[69] X. Wang, B. Xi, X. Ma, et al., Nano Lett. 20 (2020) 2899–2906.
[70] T. He, S. Weng, Y. Ye, et al., Energy Storage Mater. 38 (2021) 389–396.
[71] K. Zhu, S. Wei, H. Shou, et al., Nat. Commun. 12 (2021) 6878.
[72] J.H. Jo, Y.K. Sun, S.T. Myung, J. Mater. Chem. A 5 (2017) 8367–8375.
[73] J. Ji, H. Wan, B. Zhang, et al., Adv. Energy Mater. 11 (2020) 2003203.
[74] P. He, G. Zhang, X. Liao, et al., Adv. Energy Mater. 8 (2018) 1702463.
[75] B. Tang, G. Fang, J. Zhou, et al., Nano Energy 51 (2018) 579–587.
[76] P. He, M. Yan, X. Liao, et al., Energy Storage Mater. 29 (2020) 113–120.
[77] N.B. Mahadi, J.S. Park, J.H. Park, et al., J. Power Sources 326 (2016) 522–532.
[78] Q. Li, T.Y. Wei, K.X. Ma, et al., ACS Appl. Mater. Interfaces 11 (2019) 20888–20894.
[79] H. Jiang, W. Gong, Y. Zhang, et al., J. Energy Chem. 70 (2022) 52–58.
[80] P. Ge, L. Zhang, W. Zhao, et al., Adv. Funct. Mater. 30 (2020) 1910599.
[81] G. Yoo, B.R. Koo, H.R. An, et al., J. Ind. Eng. Chem. 99 (2021) 344–351.
[82] Q. Wei, Z. Jiang, S. Tan, et al., ACS Appl. Mater. Interfaces 7 (2015) 18211–18217.
[83] M. Du, C. Liu, F. Zhang, et al., Adv. Sci. 7 (2020) 2000083.
[84] K. Zhu, T. Wu, K. Huang, Adv. Energy Mater. 9 (2019) 1901968.
[85] Y. Tong, S. Su, X. Li, et al., J. Power Sources 528 (2022) 231226.
[86] L. Huang, Y. Xiang, M. Luo, et al., Carbon 185 (2021) 1–8.
[87] X. Wang, Y. Zhang, J. Zheng, et al., Appl. Surf. Sci. 568 (2021) 150919.
[88] P. Ge, S. Yuan, W. Zhao, et al., ACS Appl. Energy Mater. 4 (2021) 10783–10798.
[89] A. Eftekhari, M. Mohamedi, Mater. Today Energy 6 (2017) 211–229.